Supplementary Methods

Molecular Dynamics Simulations. All simulations were carried out on GROMACS (version 5.1.1)[1,2] using periodic boundary conditions in a dodecahedron with explicit water solvent. Simulations were carried out at 300K using the AMBER03[3] force field with the TIP3P water model[4]. The starting conformations of wild-type apo and cAMP-bound CAP were generated by placing crystallographic structures (PDB ID: 4N9H and 1CGP respectively)[5,6] into separate dodecahedron boxes that extended 1.0 nm from the protein surface in any direction. Starting conformations fore the S62F variant were generated using the PyMol[7] mutagenesis tool. Each system was then minimized independently with the steepest-descent algorithm until the maximum force fell below 1000 kJ/mol/min using a step size of 0.01nm and a cutoff distance of 1.2nm for the neighbor list, Coulomb interactions, and van der Waals interactions. For equilibration runs, all bonds were constrained with the LINCS algorithm[8] and virtual sites[9] were used to allow for a 4fs time step. As before, cut-offs of 1.0 nm were used for the neighbor list, Coulomb interactions, and van der Waals interactions. The Verlet cutoff scheme was used for the neighbor list, and Particle Mesh Ewald[10] was employed for the electrostatics (with a grid spacing of 0.12 nm, PME order 4, and tolerance of 1e–5). The stochastic velocity rescaling (v-scale) thermostat[11] was used to hold the temperature at 300K, and the Berendsen barostat[12] was used to bring the system to 1 bar pressure. For the production runs, the position restraint was removed and the Parrinello-Rahman barostat[13] was employed. Conformations were stored every 10 ps. For each system, three 500ns runs were conducted totaling to 1.5μs of aggregate simulation time per system.

Dihedral angles were extracted using the MDTraj Library[14] (v. 1.7). Mappings were all drawn in PyMol (version 1.7), and all figures were constructed in Inkscape (v. 0.48).

Sensitivity analysis. We varied all the cutoff values employed in the CARDS algorithm to ensure the robustness of our results. Specifically, we varied the core width from 60° to 90°, the likelihood ratio cutoff from 1.5 to 5.0, and the neighbor distance cutoff from 2 Å to 6 Å. Fig. S1 demonstrates that the communication to the CBD does not change dramatically as these parameters are varied.

References

(1) Abraham, M. J.; Murtola, T.; Schulz, R.; Páll, S.; Smith, J. C.; Hess, B.; Lindahl, E. GROMACS: High Performance Molecular Simulations Through Multi-Level Parallelism From Laptops to Supercomputers. *SoftwareX* **2015**, *1-2*, 19–25.

(2) Van Der Spoel, D.; Lindahl, E.; Hess, B.; Groenhof, G.; Mark, A. E.; Berendsen, H. J. C. GROMACS: Fast, Flexible, and Free. *Journal of Computational Chemistry* **2005**, *26* (16), 1701–1718.

(3) Duan, Y.; Wu, C.; Chowdhury, S.; Lee, M. C.; Xiong, G.; Zhang, W.; Yang, R.; Cieplak, P.; Luo, R.; Lee, T.; Caldwell, J.; Wang, J.; Kollman, P. A Point-Charge Force Field for Molecular Mechanics Simulations of Proteins Based on Condensed-Phase Quantum Mechanical Calculations. *Journal of Computational Chemistry* **2003**, *24* (16), 1999–2012.

(4) Jorgensen, W. L.; Chandrasekhar, J.; Madura, J. D.; Impey, R. W.; Klein, M. L. Comparison of Simple Potential Functions for Simulating Liquid Water. *J. Chem. Phys.* **1983**, *79* (2), 926–935.

(5) Seok, S.-H.; Im, H.; Won, H.-S.; Seo, M.-D.; Lee, Y.-S.; Yoon, H.-J.; Cha, M.-J.; Park, J.-Y.; Lee, B.-J. Structures of Inactive CRP Species Reveal the Atomic Details of the Allosteric Transition That Discriminates Cyclic Nucleotide Second Messengers. *Acta Crystallogr. D Biol. Crystallogr.* **2014**, *70* (Pt 6), 1726–1742.

(6) Schultz, S. C.; Shields, G. C.; Steitz, T. A. Crystal Structure of a CAP-DNA Complex: the DNA Is Bent by 90 Degrees. *Science* **1991**, *253* (5023), 1001–1007.

(7) DeLano, W. L. *The PyMOL Molecular Graphics System, Ver. 1.3*; Schrödinger, 2010.

(8) Hess, B. P-LINCS: a Parallel Linear Constraint Solver for Molecular Simulation. *J. Chem. Theory Comput.* **2008**, *4* (1), 116–122.

(9) Feenstra, K. A.; Hess, B.; Berendsen, H. Improving E_Ciency of Large Timescale Molecular Dynamics Simulations of Hydrogen-Rich Systems. *J Comput Chem* **1999**, *20* (8), 786–798.

(10) Essmann, U.; Perera, L.; Berkowitz, M. L.; Darden, T.; Lee, H.; Pedersen, L. G. A Smooth Particle

Mesh Ewald Method. *J. Chem. Phys.* **1995**, *103* (19), 8577–8593.
(11) Bussi, G.; Donadio, D.; Parrinello, M. Canonical Sampling Through Velocity Rescaling. *J. Chem. Phys.* **2007**, *126* (1), 014101.
(12) Berendsen, H. J. C.; Postma, J. P. M.; van Gunsteren, W. F.; DiNola, A.; Haak, J. R. Molecular Dynamics with Coupling to an External Bath. *J. Chem. Phys.* **1984**, *81* (8), 3684–3690.
(13) Parrinello, M.; Rahman, A. Polymorphic Transitions in Single Crystals: a New Molecular Dynamics Method. *Journal of Applied Physics* **1981**, *52* (12), 7182–7190.
(14) McGibbon, R. T.; Beauchamp, K. A.; Harrigan, M. P.; Klein, C.; Swails, J. M.; Hernández, C. X.; Schwantes, C. R.; Wang, L.-P.; Lane, T. J.; Pande, V. S. MDTraj: a Modern Open Library for the Analysis of Molecular Dynamics Trajectories. *Biophysical Journal* **2015**, *109* (8), 1528–1532.

Supplemental Figures

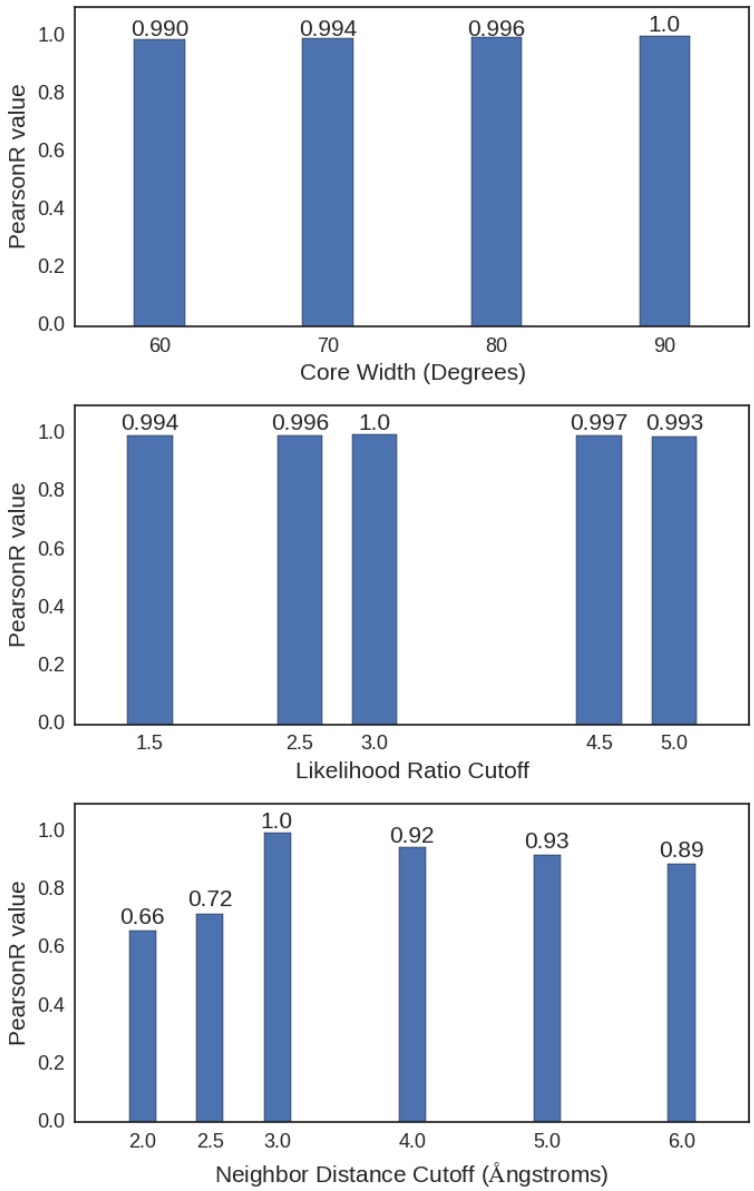

Supporting Figure 1. Pearson Correlation Coefficients (PearsonR) between the CARDS results presented in the main text and those with varying **A.** the core width, **B.** the likelihood ratio cutoff, and **C.** the neighbor distance cutoff.

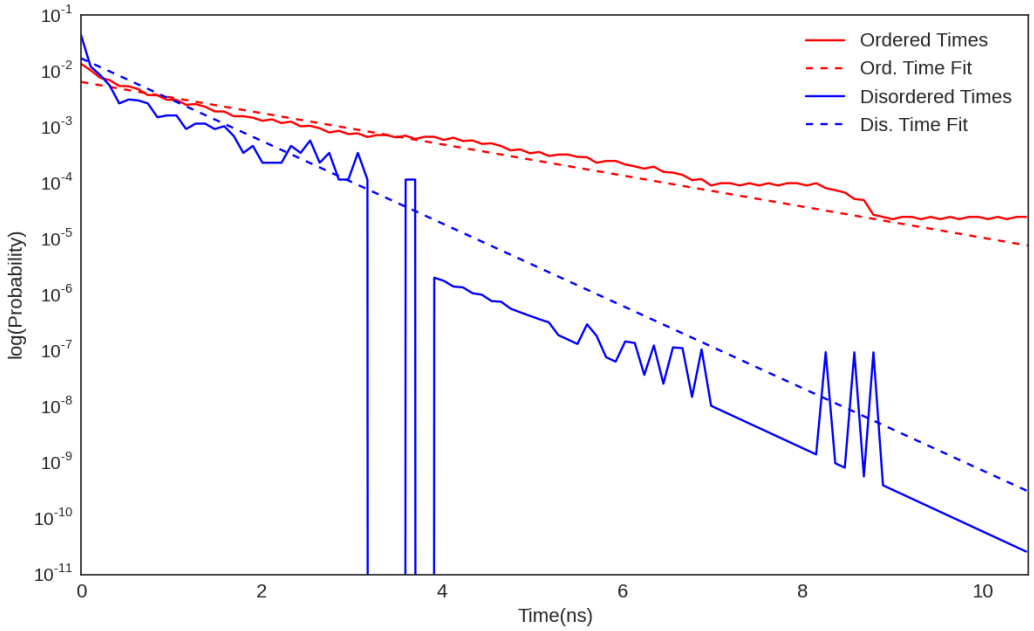

Supporting Figure 2. The distribution of ordered and disordered times for a single dihedral across a single simulation trajectory. The solid lines represent the histogram of times extracted from the trajectory, while the dashed lines represent fits based on the average ordered ($\langle\tau_{ord}\rangle$) and disordered times ($\langle\tau_{dis}\rangle$).

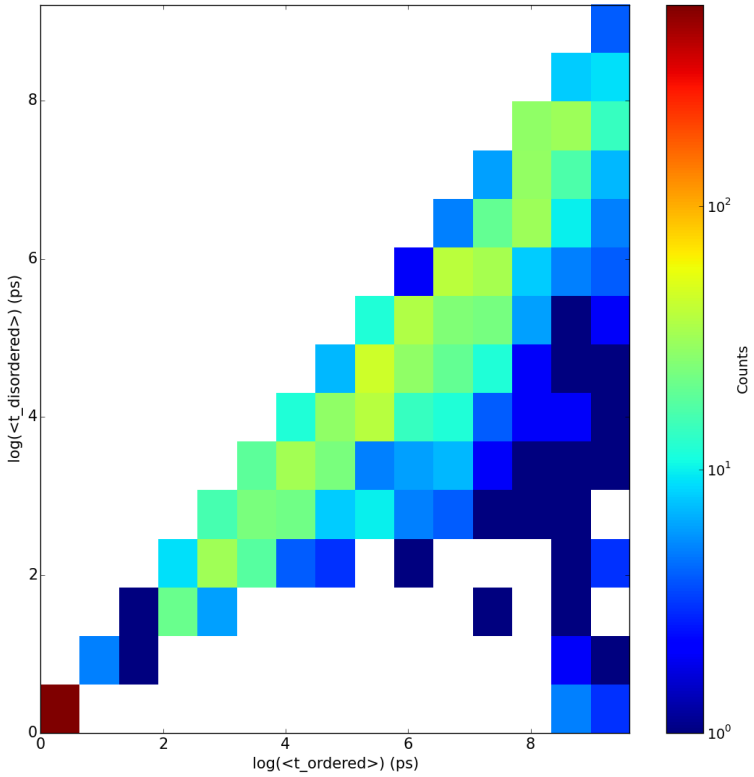

Supporting Figure 3. Two-dimensional histogram of the average ordered and disordered times ($\langle\tau_{ord}\rangle$ and $\langle\tau_{dis}\rangle$) for all dihedrals in CAP.

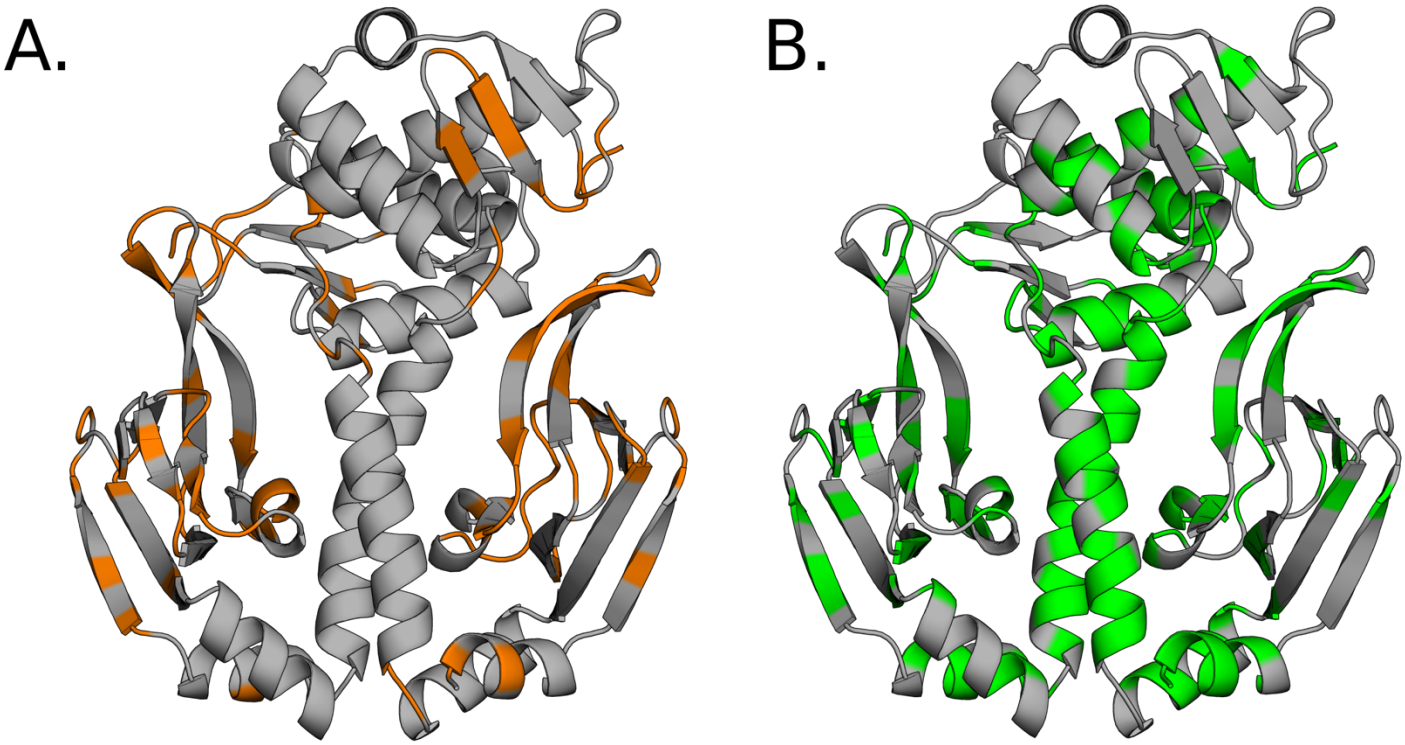

Supporting Figure 4. Residues with separable dihedrals into disordered regimes using a stricter threshold ($\langle\tau_{ord}\rangle \geq 5\times\langle\tau_{dis}\rangle$). **A.** Residues with at least one backbone dihedral that is capable of disorder-mediated communication (orange). **B.** Residues with at least one side-chain dihedral that is capable of disorder-mediated communication (green).

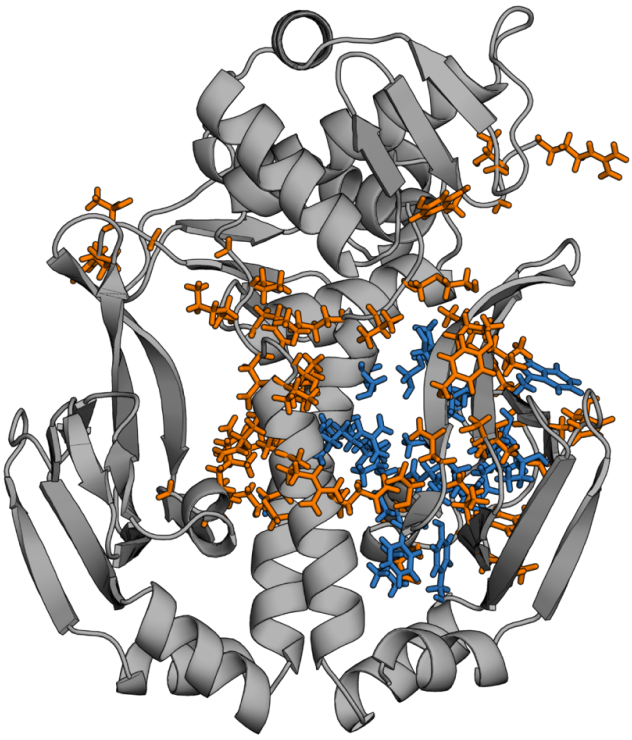

Supporting Figure 5. The top 5% of residues (orange sticks) with disorder-mediated communication to the cAMP-binding pocket (blue sticks). Note that having disorder-mediated communication to the CBD does not preclude the possibility of also having structural communication.

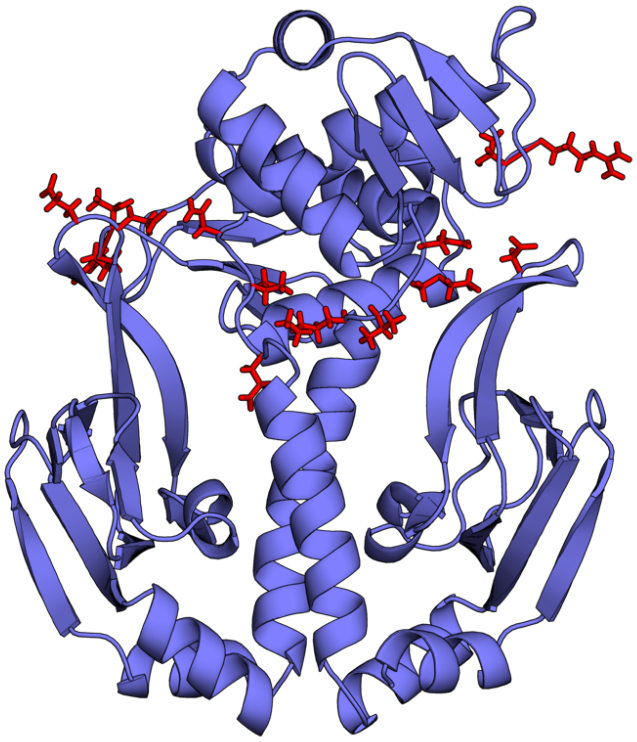

Supporting Figure 6. The top 2% of backbone-side-chain hubs (sticks).

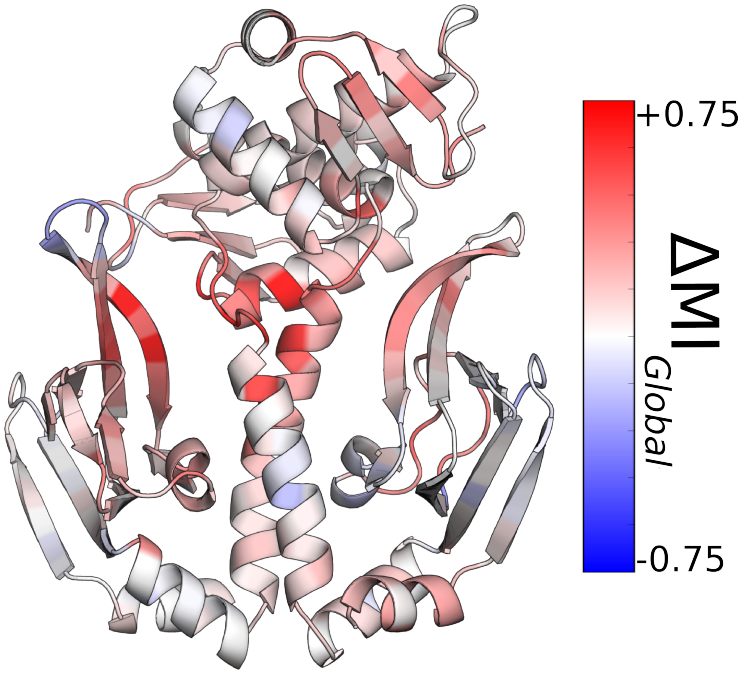

Supporting Figure 7. Change in global communication upon the S62F mutation. The color scale on the right shows the proportional change in global communication relative to the scale in Figure 7 of the main text.